# *Volcanic Ash Detection: ATBD*

Doc.No. : EUM/MET/REP/07/0467
Issue : v2
Date : 15 May 2014
WBS/DBS :

EUMETSAT
Eumetsat-Allee 1, D-64295 Darmstadt, Germany
Tel: +49 6151 807-7
Fax: +49 6151 807 555
http://www.eumetsat.int

## *Document Change Record*

| *Issue / Revision* | *Date* | *DCN. No* | *Changed Pages / Paragraphs* |
|---|---|---|---|
| Version 1A | 14/11/2007 | | First Release |
| Version 2 | 15/05/2014 | | Updated template, signature table and content review. |

# *Table of Contents*



# *Table of Figures*



# *Table of Tables*

# 1 INTRODUCTION

## 1.1 Purpose and Scope

Volcanic ash plumes can affect public health in the surrounding regions and have a hazardous impact on air traffic. An early detection and continuous monitoring of the ash plumes plays a key role for air traffic safety.

The current generation of Meteosat satellite (Meteosat econd Generation, MSG) is not only monitoring parts of the Earth disc every 15 minutes, but its channels can also identify and separate ash plumes from other clouds. Therefore MSG and the volcanic ash detection algorithm can support the volcanic ash plumes monitoring activities.

## 1.2 Document Structure

In the following, chapter 2 gives an overview of the MSG imaging instrument SEVIRI (Spinning Enhanced Visible and Infrared Radiometer), the general approach for the volcanic ash detection, and the description of the algorithm together with the practical application of the tests and the algorithm. In chapter 3 a few results are discussed.

## 1.3 Reference Documents

| *Number* | *Author and name* | *Reference* |
|---|---|---|
| RD 1 | Ellrod G., B. Connell, and D. Hillger, 2003: *Improved detection of airborne volcanic ash using multi-spectral infrared satellite data.* | Journal Geophysical. Research, 108 (D12), 4356. |
| RD 2 | Loveland T.R. and Belward A.S., 1997 *The IGBP-DIS global 1km land cover data set, DISCover: first results.* | Int. Journal of Remote Sensing, Vol. 18, No. 15, pp. 3289 |
| RD 3 | Lutz H.J., 1999: *Cloud processing for Meteosat Second Generation* | EUMETSAT Technical Memorandum No. 4 |
| RD 4 | Lutz H.J., 2007: Cloud Detection for MSG – Algorithm Theoretical Basis Document (ATBD). | EUM/MET/REP/07/0132 |
| RD 5 | Pavolonis, M. J., W. F. Feltz, A. K. Heidinger, and G. M. Gallina, 2006: *A daytime complement to the reverse absorption technique for improved automated detection of volcanic ash.* | Jorunal of Atmospheric and Oceanic Tech., Vol. 23, pp.1422 |
| RD 6 | Prata, F., 1989: *Observations of volcanic ash clouds in the 10-12 $\mu$m window using AVHRR/2 data.* | International Journal of Remote Sensing, 10, 751-761. |
| RD 7 | Prata F., A. Schreiner, T. J. Schmit, and G. P. Ellrod, 2004: *First measurements of volcanic sulfur dioxide from the GOES Sounder: Implications for improved aviation safety* | Proceedings, Second International Conference on Volcanic Ash and Aviation Safety, 21-24 June 2004, Alexandria, Virginia, Paper number 3.7. |

# 2 ALGORITHM DESCRIPTION

## 2.1 Physics of the problem

Volcanic ash plumes have been monitored with geostationary satellite images since the late 1970s. However, the use of single-band infrared and visible images makes it difficult to distinguish between ash plumes and thin cirrus clouds or even the underlying surface. Prata (1989) introduced the "split-window", for ash cloud detection, a technique also called "reverse absorption" technique. This technique uses the fact that the absorption of clouds (ice and water) is higher in channel IR12.0 than in IR10.8, but the opposite for ash plumes. See Figure 1.

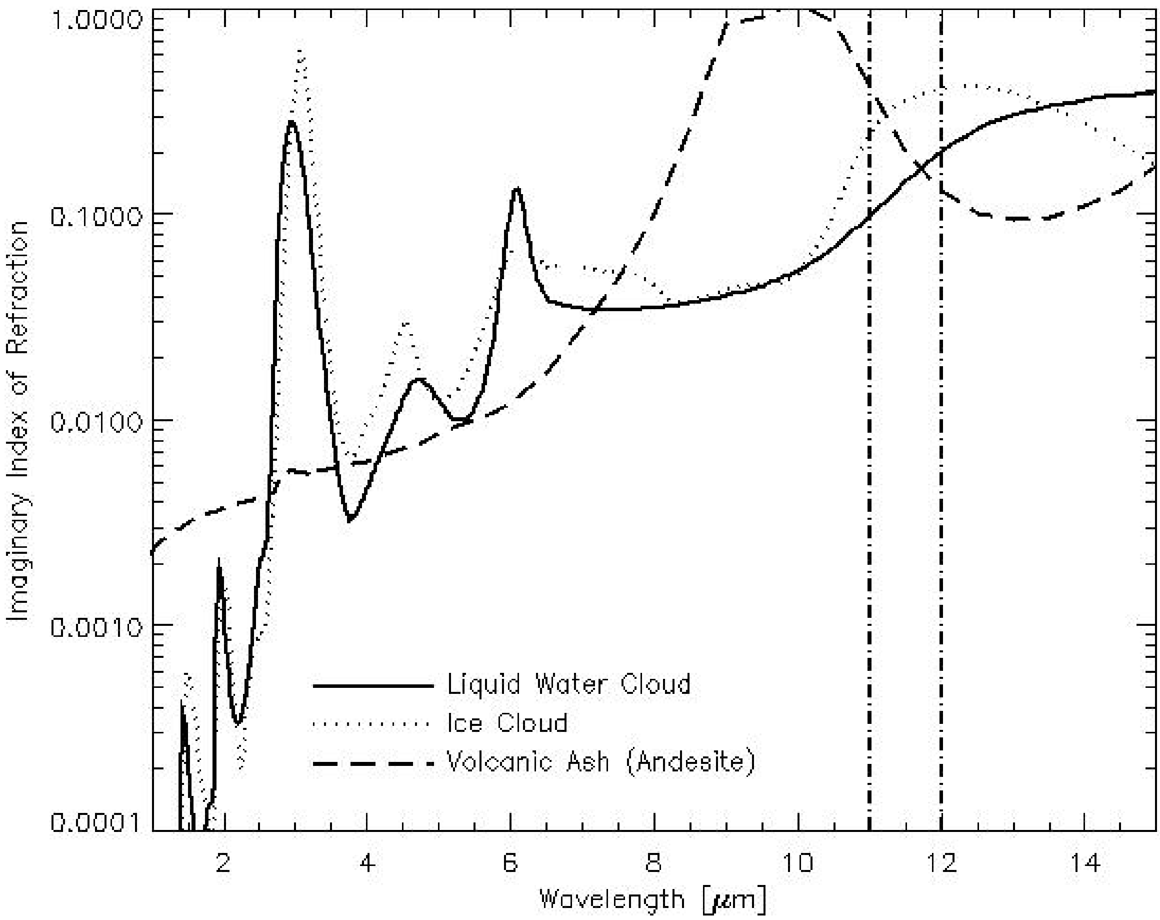


*Figure 1: Imaginary index of refraction of ash, water and ice clouds*

However, the split window method has still some deficiencies detailed in [RD 1].

- Opaque ash clouds are still hard to distinguish from ice or water clouds, and ash clouds are often opaque within the first few hours of the eruption
- ice embedded in the eruption cloud may obscure the ash signal
- In moist atmospheres (tropics) low level ash clouds may be masked by water vapour absorption effects.

With the new geostationary satellites like MSG, additional multi-spectral approaches can be tested to support and improve the "split-window" technique. For example some constituents of the ash clouds such as sulfur dioxide ($SO_2$) or sulfates can be detected in addition by channels in the 3.9 µm and 8.7 µm bands, MSG channels IR3.9 and IR8.7 See also RD 1 and RD 5.

In addition to the IR channels, the visible channels can be used during daylight. As shown in Figure 2, the single scattering albedo of water and ice clouds decrease with higher wavelength, while the single scattering albedo of ash cloud increase or at least is stable. Using the ratio of the solar contribution in channel IR3.9 with the visible channel VIS0.6, ash clouds can be separated from ice or water clouds.

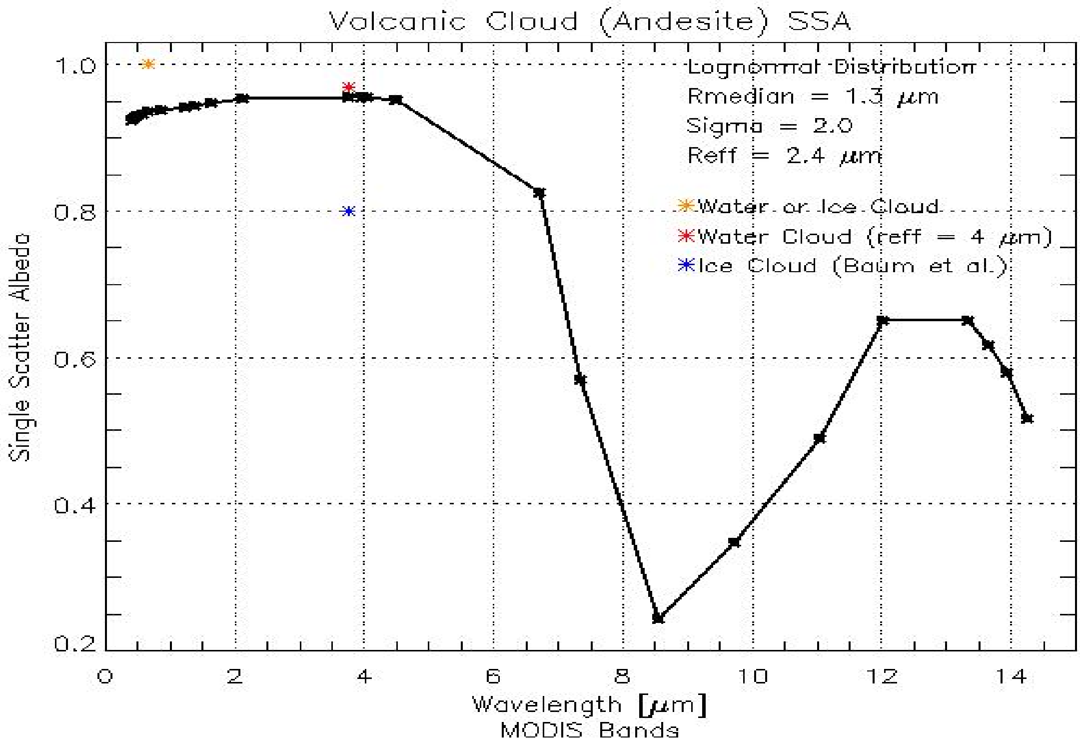


*Figure 2: Single-scattering albedo of volcanic ash and of water and ice clouds*

The spectral characteristics of MSG SEVIRI with its 12 channels (see Table 1) and its high spatial and temporal resolution (3 km at the sub-satellite point, 15 minute image repeat cycle) are thus highly useful for the detection of volcanic ash clouds.

The new MSG volcanic ash cloud detection algorithm (VOL) makes use of the MSG channels 1 (VIS0.6), 4 (IR3.9), 6 (WV7.3), 7 (IR8.7), 9 (IR10.8), 10 (IR12.0) and 11 (IR13.4).

Table 1 shows the characteristics of the twelve MSG-SEVIRI channels.

| *Channel* | *Central wavelength (µm)* | *Spectral band (µm)* |
|---|---|---|
| VIS 0.6 | 0.635 | 0.56–0.71 |
| VIS 0.8 | 0.81 | 0.74 - 0.88 |
| IR 1.6 | 1.64 | 1.50 - 1.78 |
| IR 3.9 | 3.92 | 3.48 - 4.36 |
| IR 8.7 | 8.70 | 8.30 - 9.10 |
| IR 10.8 | 10.8 | 9.80 - 11.80 |
| IR 12.0 | 12.0 | 11.00 - 13.00 |
| WV 6.2 | 6.25 | 5.35 - 7.15 |
| WV 7.3 | 7.35 | 6.85 - 7.85 |
| IR 9.7 | 9.66 | 9.38 - 9.94 |
| IR 13.4 | 13.40 | 12.40 - 14.40 |
| HRV | 0.75 | Broadband visible |

*Table 1: Characteristics of the MSG-SEVIRI channels*

In addition to the detection of ash, it is also possible to detect $SO_2$ with the help of MSG channels IR9.7 and WV7.3 [RD 7]. This may be important to estimate climatic effects and detect volcanic activities. However, due to the difference in weight and density between the solid ash particles and the gaseous $SO_2$ cloud, they may be transported into different altitudes and thus also into different directions. Because of the intention to support the aircraft security, the described MSG algorithm tries only to detect and monitor the more dangerous ash clouds and has no additional $SO_2$ detection implemented.

## 2.2 Mathematical Description of the Algorithm

As implemented in the operational processing chain, the volcanic ash detection algorithm (VOL) is only applied to cloud pixels, as detected by the scenes analysis [RD 4]. For the detected cloud pixels, the VOL algorithm uses the following criteria to check for ash cloud pixels:

- Reflectance ratio IR3.9(solar component)/VIS0.6 (daylight and twilight only)
- Brightness temperature difference of channels IR3.9 and IR10.8 (night only)
- Brightness temperature difference of channels IR8.7 and IR10.8
- Brightness temperature difference of channels IR12.0 and IR10.8

The main two tests for ash cloud detection are the reflectance ratio test IR3.9(solar)/VIS0.6 and the brightness temperature difference test of channels IR12.0 and IR10.8. While the reflectance ratio test can almost clearly separate all ash clouds from other clouds, the brightness temperature difference test IR12.0 - IR10.8 may have similar differences for thin ice and water clouds as for ash clouds. For that reason, there is a need to filter out wrongly classified ash clouds/ice clouds during night, when the reflectance ratio test cannot be used. Therefore, the algorithm uses the two further brightness temperature difference tests.

### 2.2.1 Input datasets

The VOL algorithm uses the following input data:

- satellite data,
- cloud mask (derived by the SCE algorithm)
- Radiative Transfer Model output (e.g. RTTOV) using ECMWF forecast data
- auxiliary data (see section 2.4).

The algorithm uses MSG channels VIS0.6, IR3.9, IR8.7, IR10.8, IR12.0 and IR13.4. From the radiances of channels IR3.9, IR10.8, IR13.4 and the solar zenith angle, the reflectance of channel IR3.9 (refl3.9) is calculated.

The cloud mask derived from the Scenes Analysis (SCE) provides the cloudy pixels. A description of the SCE algorithm is given by [RD 3] and [RD 4].

The auxiliary datasets are described in chapter 2.4.

### 2.2.2 Description of the threshold tests

The algorithm checks if the cloud pixel is within a 5 º circle around the location of a volcano (location is given in static dataset). The solar zenith angle is checked for day (solar zenith angle < 80°), night (solar zenith angle > 90°) or twilight (angle between 80 ° and 90 °) conditions in order to select the appropriate thresholds and tests. The algorithm itself is based on a simple threshold algorithm.

| During daylight hours, a pixel is identified as volcanic ash, if the following criteria are matched: |
| --- |
| The temperature difference IR8.7 - IR10.8 is larger than threshold 1 |
| The temperature difference IR12.0 - IR10.8 is larger than threshold 2 |
| The reflectance ratio IR3.9(solar) / VIS0.6 is larger than threshold 3 |

| During twilight, a pixel is identified as volcanic ash, if the following criteria are matched: |
| --- |
| The temperature difference IR8.7 - IR10.8 is larger than threshold 1 |
| The temperature difference IR12.0 - IR10.8 is larger than threshold 2 |
| The reflectance ratio IR3.9(solar) / VIS0.6 is larger than threshold 4 |
| The temperature difference IR3.9 - IR10.8 is between threshold 5 and threshold 6 |

| During hours of darkness, a pixel is identified as volcanic ash if the following criteria are matched: |
| --- |
| The temperature difference IR8.7 - IR10.8 is larger than threshold 1 |
| The temperature difference IR12.0 - IR10.8 is larger than threshold 2 |
| The temperature difference IR3.9 - IR10.8 is between threshold 7 and threshold 8 |

### 2.2.3 Derivation of the thresholds

The thresholds used to perform the above described tests are derived as follows:

$$\text{Threshold1} = a_{1,1} + a_{2,1} * T_{PCS,8.7} + a_{3,1} * T_{PCS,10.8}$$
$$\text{Threshold2} = a_{1,2} + a_{2,2} * T_{PCS,12.0} + a_{3,2} * T_{PCS,10.8}$$
$$\text{Threshold3} = a_{1,3}$$
$$\text{Threshold4} = a_{1,4}$$
$$\text{Threshold5} = a_{1,5} + a_{2,5} * T_{PCS,3.9} + a_{3,5} * T_{PCS,10.8}$$
$$\text{Threshold6} = a_{1,6} + a_{2,6} * T_{PCS,3.9} + a_{3,6} * T_{PCS,10.8}$$
$$\text{Threshold7} = a_{1,7} + a_{2,7} * T_{PCS,3.9} + a_{3,7} * T_{PCS,10.8}$$
$$\text{Threshold8} = a_{1,8} + a_{2,8} * T_{PCS,3.9} + a_{3,8} * T_{PCS,10.8}$$

with ($T_{PCS,chan}$ ) denoting the predicted clear sky brightness temperature in channel *chan* derived from the ECMWF forecast with the radiative transfer model.

The coefficients a are listed in Table 2:

| Threshold | $\mathbf{a_{1,x}}$ | $\mathbf{a_{2,x}}$ |
| --- | --- | --- |
| Threshold1 | 3.0 | 1.0 |
| Threshold2 | 2.0 | 1.0 |
| Threshold3 | 1.3 | |
| Threshold4 | 1.5 | |
| Threshold5 | 4.0 | 1.0 |
| Threshold6 | 10.0 | 1.0 |
| Threshold7 | 0.0 | 1.0 |
| Threshold8 | 8.0 | 1.0 |

*Table 2: Coefficients to derive the VOL thresholds*

In addition to the ash cloud detection, the location of the volcano is checked to detect the hotspot caused by the eruption. This is done by checking the pixel at volcano location and its neighbouring pixels as follows: A pixel is a hotspot

- if the brightness temperature in channel IR3.9 is larger than 300 K and if the standard deviation of channel IR3.9 (3x3 pixel) is larger than 4 K,
- or if the brightness temperature in channel IR3.9 is larger than 320 K and if the standard deviation of channel IR3.9 (3x3 pixel) is larger than 2.5 K

## 2.3 Assumptions, Constraints, and Limitations

The current volcanic ash detection algorithm is able to detect volcanic ash clouds with a minimum of false classifications at daytime. However, ash plume detection during hours of darkness still remains challenging.

## 2.4 Auxiliary Datasets

The VOL algorithm uses the following auxiliary dataset:

- Pixel-based land-sea-mask/surface-type-map
- ECMWF forecast data.
- List with locations of active volcanoes. See also Figure 3)

The pixel-based land-sea-mask/surface-type-map consists of 17 different land surface types and one ocean/open water surface type. This map has been derived from the International Geosphere-Biosphere Programme (IGBP) surface type map [RD 2].

The list of active volcanoes contains currently 14 entries, where some of these represent entire groups of neighbouring volcanoes.

# 3 RESULTS

The algorithm was applied to Meteosat-8 data of 25 November 2005, when the Karthala volcano erupted. This volcano forms most of the landmass of Grande Comore (also called Ngazidja), the main island of the Union of the Comoros. It is situated at 11.75 S and 43.38 E in the Indian Ocean and is one of the largest active volcanoes in the world. The first eruptions started at around 1800 UTC on 24 November 2005. At around 0500 UTC, the ash plume darkened the sky to conditions like in the late evening with ash deposits on the grounds of as much as 10 centimetres. Very significant amounts of dust and ash were released during this eruption, which were largely carried to the south-west area of the island. Several international flights and several local flights were cancelled during the period 26-27 November 2005.

To demonstrate the capability of the VOL algorithm, the situation on 25 November 2005 at 12 UTC is shown as an example. Figure 3.1 shows all locations of the current active volcanoes within the Meteosat field of view. The location of the Karthala volcano near Madagascar is marked by a black x.

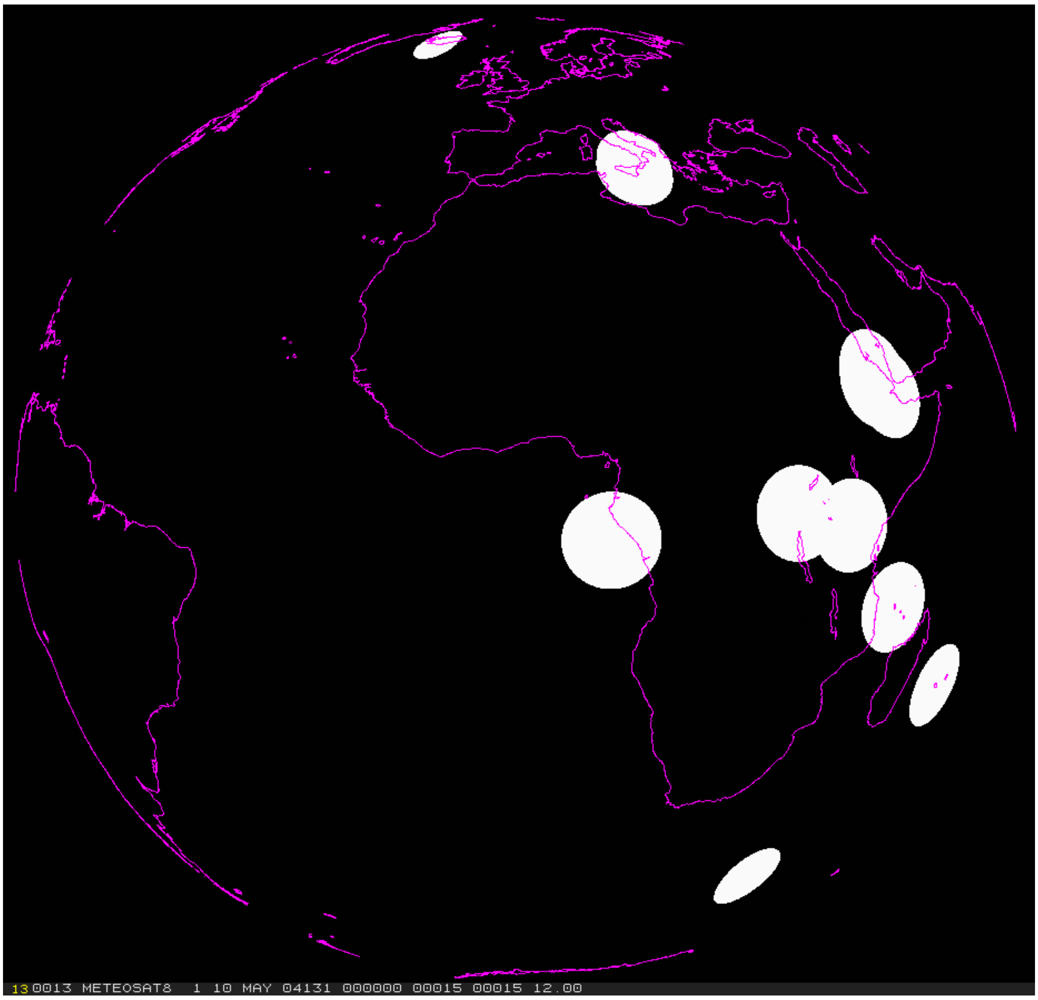


*Figure 3: Location and size of the ash detection processing area.*

Figure 4 shows channel IR10.8 of Meteosat-8 on 25 November 2005 at 1200 UTC. The area of the volcano and the ash cloud is marked by a red circle. In this figure, warm areas appear dark and cold areas appear bright. The ash plume appears colder than the low level clouds and the clear surface, but it is warmer than the cloud tops of the highest clouds. In this case, the ash plume has brightness temperatures similar to the surrounding semi-transparent ice clouds.

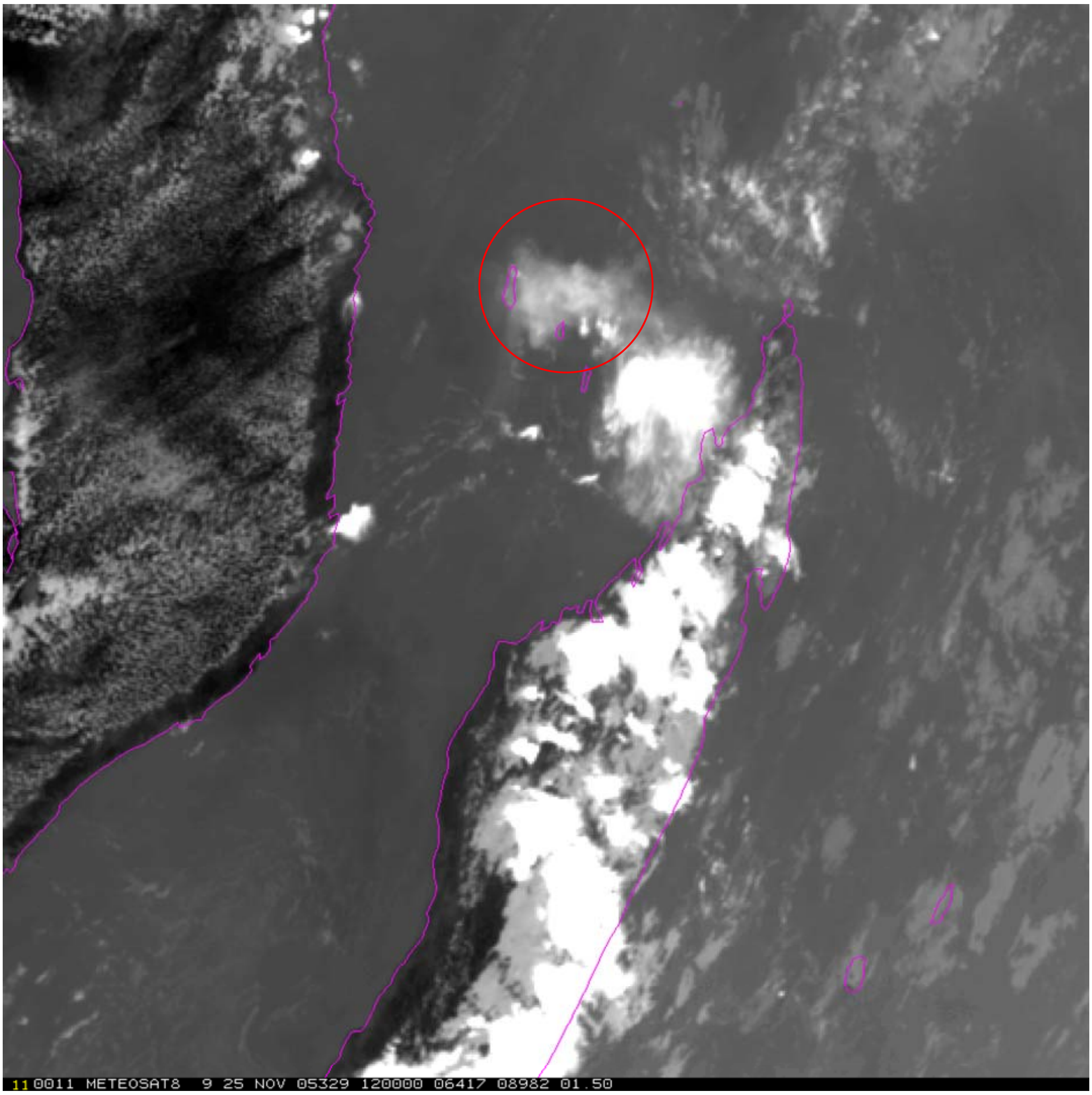


*Figure 4: Channel IR10.8 brightness temperatures on 25 November 2005 at 12 UTC. Bright means low temperatures, dark means high temperatures. The position of the volcano Karthala and the ash plume is marked by the red circle.*

Figure 5 shows the difference of channels IR8.7 and IR10.8 of Meteosat-8 on 25 November 2005 at 1200 UTC. The area of the volcano and the ash cloud is marked by a red circle. Again, the ash plume appears similar to the surrounding ice clouds.

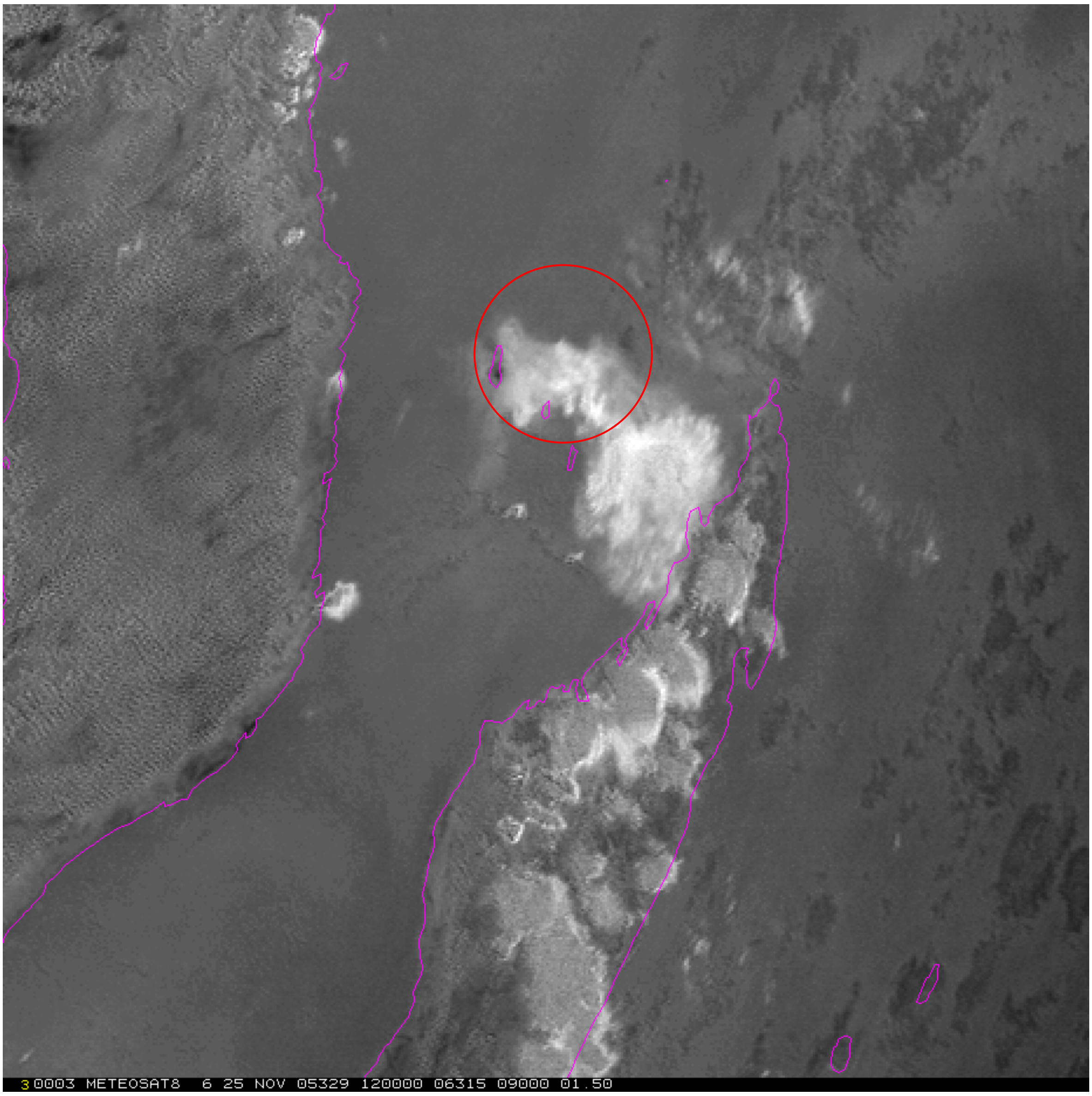


*Figure 5: Difference of channel IR8.7 and IR10.8. Bright means that IR8.7 is warmer than IR10.8. The position of the volcano Karthala and the ash plume is marked by the red circle.*

Figure 6 shows the difference of channels IR12.0 and IR10.8 of Meteosat-8 on November 25, 2005 at 1200 UTC. The area of the volcano and the ash cloud is marked by a red circle. For this difference, the ash plume appears much brighter than normal clouds, which means that the ash plume channel IR12.0 is warmer than channel IR10.8. See also Figure 1.

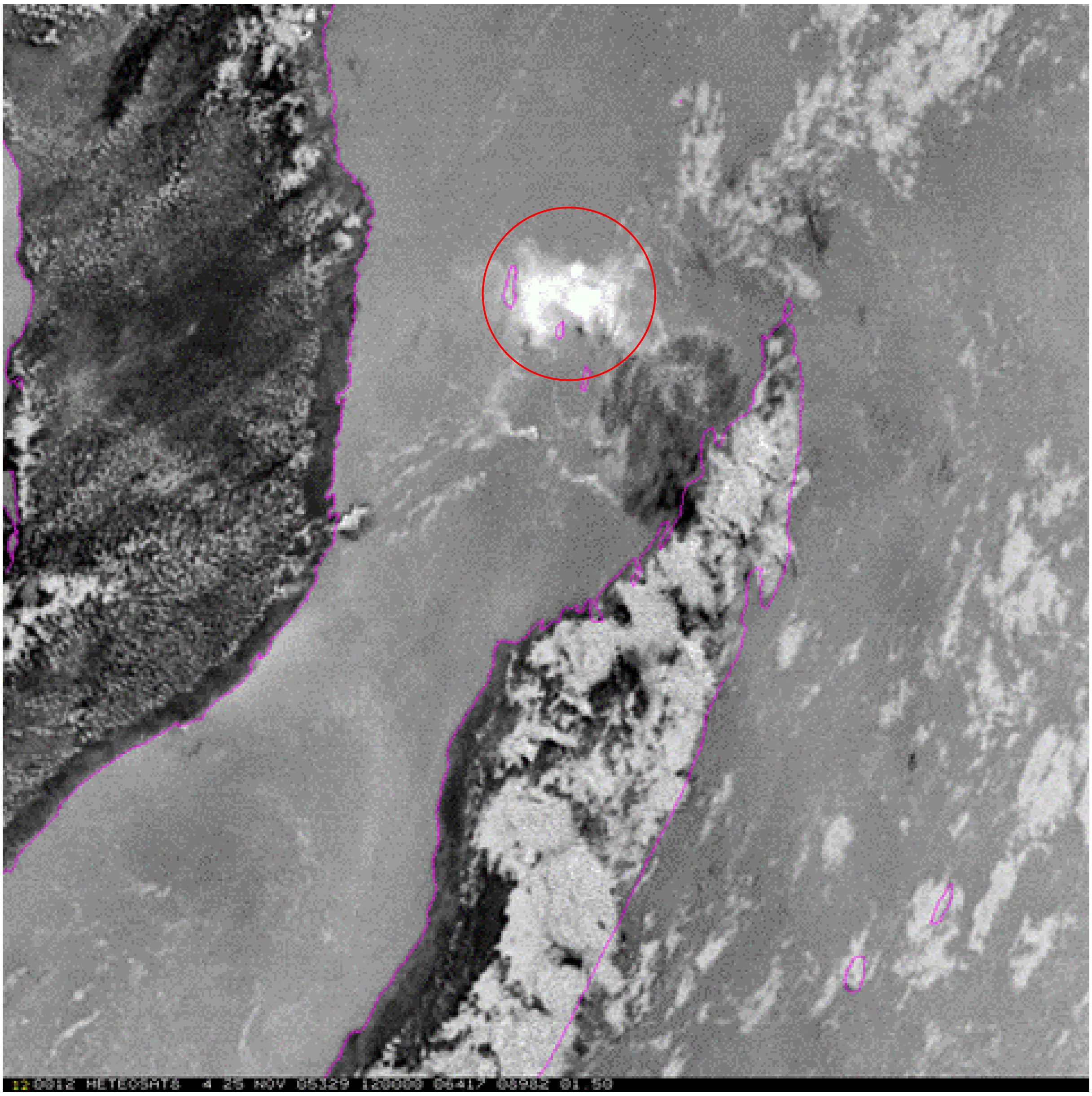


*Figure 6: Difference of channel IR12.0 and IR10.8. Bright means that IR12.0 is warmer than IR10.8. The position of the volcano Karthala and the ash plume is marked by the red circle.*

Figure 7 shows the ratio of the solar part of channel IR3.9 and channel VIS0.6 of Meteosat-8 on November 25, 2005 at 1200 UTC. The area of the volcano and the ash cloud is marked by a red circle. In this comparison, the ash plume appears much brighter than normal clouds, which means that the ash plume has higher reflectances in channel IR3.9 than in channel VIS0.6. See also Figure 2. Clouds appear dark, cloud-free land appears bright. In this test, the ash plume can easily be separated from other clouds.

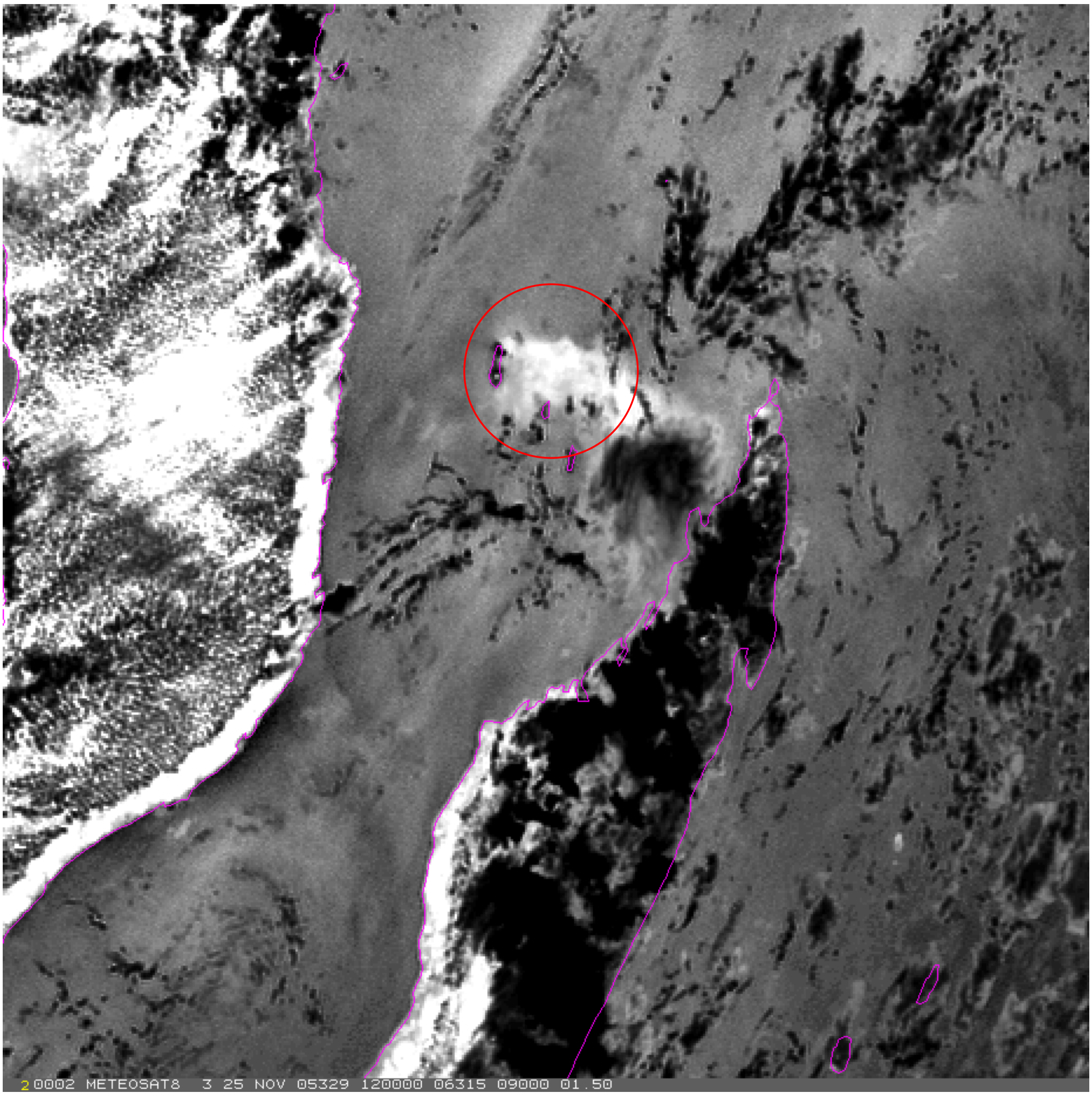


*Figure 7: Ratio of the solar part of channel IR3.9 with channel VIS0.6. Bright means that that the reflectance in IR3.9 is higher than in channel VIS0.6 The position of the volcano Karthala and the ash plume is marked by the red circle.*

Figure 8 shows the result of the ash plume detection algorithm for Meteosat-8 on 25 November 2005 at 1200 UTC. The processing area of the ash cloud detection can be seen by the different brightness of the detected clouds within the area (grey) and outside the area (white). The ash plume itself is orange.

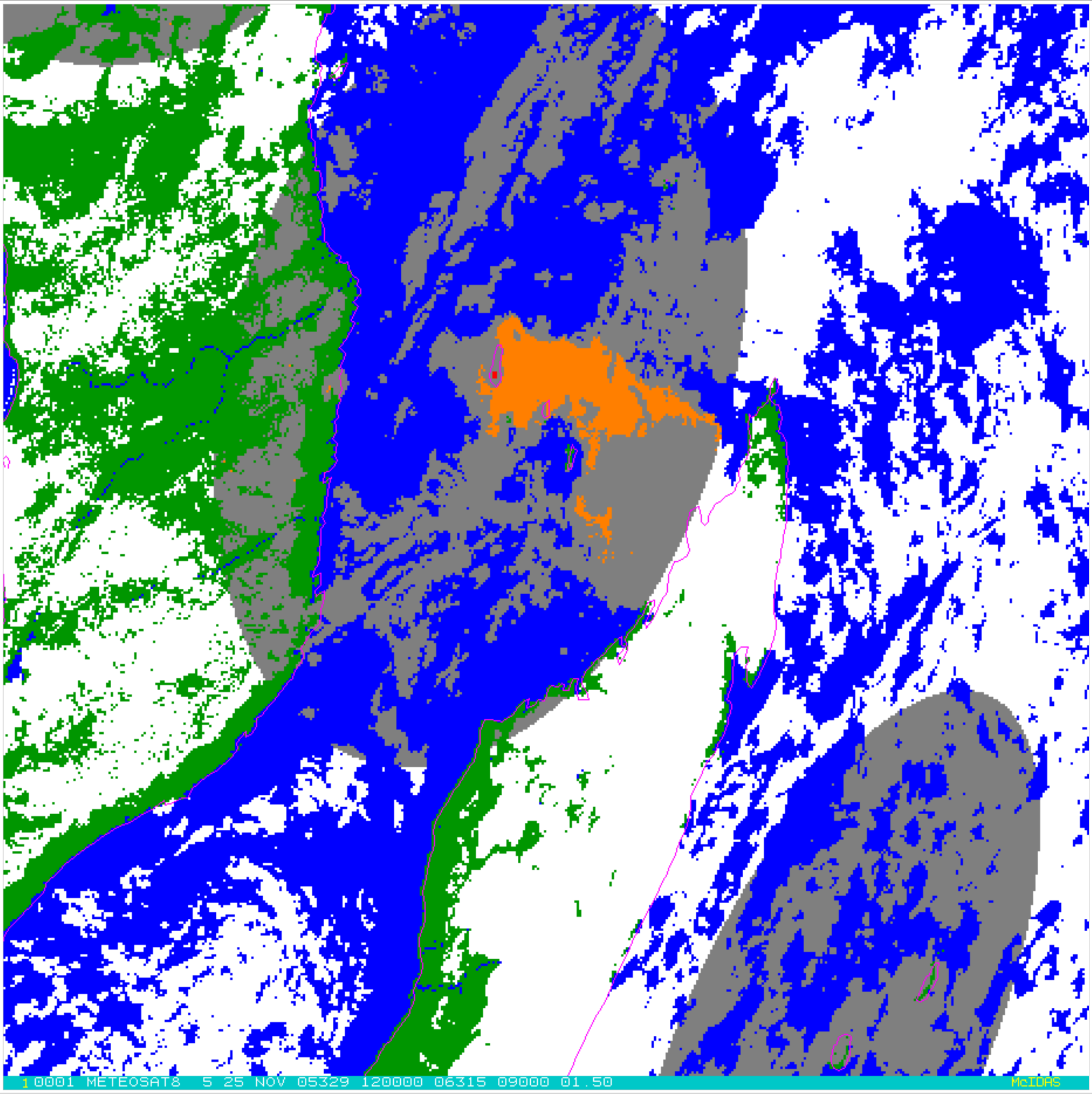


*Figure 8: Results of the ash plume detection. The red dot on the island marks the detected hotspot of the volcano. The table below explains the colour coding:*

| | |
|---|---|
| Blue | clear ocean |
| Green | clear land |
| White | clouds |
| Grey | clouds within the search area |
| Orange | ash plume |